Photon echo spectroscopy reveals structure-dynamics relationships in carotenoids

N. Christensson,[1] T. Polivka,[2,3] A. Yartsev,[1] and T. Pullerits[1]
[1]*Department of Chemical Physics, Lund University, Box 124, SE-21000, Lund, Sweden*
[2]*Institute of Physical Biology, University of South Bohemia, Nove Hrady, Czech Republic*
[3]*Institute of Plant Molecular Biology, Biological Center, Czech Academy of Sciences, Ceske Budejovice, Czech Republic*
(Received 29 December 2008; revised manuscript received 27 April 2009; published 17 June 2009)

Based on simultaneous analysis of the frequency-resolved transient grating, peak shift, and echo width signals, we present a model for the third-order optical response of carotenoids including population dynamics and system-bath interactions. Our frequency-resolved photon echo experiments show that the model needs to incorporate the excited-state absorption from both the S_2 and the S_1 states. We apply our model to analyze the experimental results on astaxanthin and lycopene, aiming to elucidate the relation between structure and system-bath interactions. Our analysis allows us to relate structural motifs to changes in the energy-gap correlation functions. We find that the terminal rings of astaxanthin lead to increased coupling between slow molecular motions and the electronic transition. We also find evidence for stronger coupling to higher frequency overdamped modes in astaxanthin, pointing to the importance of the functional groups in providing coupling to fluctuations influencing the dynamics in the passage through the conical intersection governing the S_2-S_1 relaxation.

DOI: 10.1103/PhysRevB.79.245118 PACS number(s): 78.20.Bh, 78.47.Fg, 82.20.Sb, 82.53.Kp

I. INTRODUCTION

Since the dawn of ultrafast spectroscopy, excited-state dynamics of molecules in condensed phase has been the subject of a vast number of experiments aiming to disentangle relaxation processes in various molecules. The majority of studies utilized transient absorption or fluorescence up-conversion that both can follow electronic and vibrational population dynamics. These dynamics of the system are inherently related to the system-bath interaction. The information about the above-mentioned interaction can be obtained from the pump-probe signal,[1] but separating it from the population dynamics is difficult. The majority of experiments have been performed with ~100 fs pulses, thereby scrambling the signals related to the system dynamics with the information of the system-bath interaction. Yet, the system-bath interaction is crucial for understanding the energy dissipation during the relaxation of the system. The rapid development of ultrafast spectroscopy in the last decade promoted development of coherent multipulse methods particularly sensitive to the coupling between the system and bath degrees of freedom.[2–6] The most common are various types of four-wave mixing schemes, among which the three-pulse photon echo peak shift[5,7] and transient grating have proved to be especially useful for studies of excited-state dynamics of molecules in condensed phase because they provide complementary information about population dynamics (transient grating) and system-bath interaction (the peak shift). These methods have been successfully applied to study solvation dynamics,[3–5,8–13] isomerization,[14] exciton relaxation, and energy transfer in photosynthetic complexes[15,16] and complex molecules and polymers.[17–22] Recently, transient grating spectroscopy has been also applied to study excited-state processes in carotenoids.[23–28]

Carotenoids are a family of naturally occurring pigments that share a polyenelike motif in their structure.[29] In the past decade, carotenoid excited-state dynamics has attracted much attention and a number of theoretical and experimental studies addressed questions concerning relaxation pathways and their dependence on carotenoid structure and solvent.[30] The interest in such studies is largely stimulated by a complicated excited-state structure which, besides the strongly allowed transitions from the ground state, also involves a few symmetry-forbidden "dark" states. Due to the polyenic structure of the conjugated chain (that assorts carotenoids to the C_{2h} point symmetry group), the absorbing state of B_u^+ symmetry is not the lowest-excited state. Instead, the excited state with A_g^- symmetry, into which the transition from the ground state is forbidden, lies for all carotenoids below the B_u^+ state. Therefore, the strong B_u^+ state is denoted S_2 and the lowest-excited electronic state, A_g^-, is commonly denoted as the S_1 state. In carotenoids with sufficiently long conjugation ($N>10$) there may be a few other dark states located within the S_2-S_1 energy gap.[30–32] Consequently, excitation of the carotenoid results in a cascade of internal conversion processes which may involve dark state(s) located below the absorbing state. Disentangling of the relaxation pathways is essential for understanding the details of the two key functions of carotenoids in nature—light harvesting and photoprotection. Since most of the carotenoids acting as light harvesting or protecting pigments have long conjugated chain and are embedded in a protein, resolving the network of relaxation pathways and revealing the effects of environment on excited-state dynamics are of high importance for understanding molecular actions of carotenoids.

Application of the four-wave mixing spectroscopy to carotenoids has been so far limited to β carotene and its derivatives.[23,24,26–28] The pioneering work carried out by Siebert *et al.*[25] applied transient grating to monitor vibrational coupling between S_1 and S_0 states, but limited time resolution prevented to draw conclusions about the S_2-S_1 relaxation. Later, degenerate four-wave mixing (DFWM) scheme using 16 fs pulses enabled to follow wave-packet dynamics in the ground state of β carotene.[28] Adding a pump pulse to

the DFWM scheme further extended the experiment to study vibrational relaxation in the S_1 state.[27,28] These studies showed that while the dephasing of the ground-state vibrations takes place on the time scale of a few picoseconds, the coherence of the S_1 vibrations is lost within ~ 100 fs. It was also concluded that the vibrational coherence is not preserved during the S_2-S_1 relaxation.[27,28] Vibrational dynamics of β carotene has also been studied by transient grating[23,24,26] and femtosecond Raman spectroscopy.[33,34] These works further confirmed the long-lived vibrational coherence in the ground state. Theoretical modeling of the transient grating signal[24] showed that the S_2-S_{n2} transition was crucial to explain the observations, but no other transition originating either from the S_1 or any intermediate state between S_2 and S_1 was needed to explain the results.[33,35] In contrast, transient absorption data supported by assignments of the intermediate states from resonance Raman profiles and/or fluorescence spectroscopy of various carotenoids has been interpreted in terms of relaxation involving more intermediates.[31] These relaxation schemes suggest that the dark states with B_u^- and A_g^- symmetry participate in the S_2-S_1 relaxation pathway for carotenoids with $N>10$.[31] The assignment of spectral signatures of these intermediates in those works relied on identification of various transient absorption bands. Such assignment is complicated especially in the red tail of the carotenoid absorption spectrum where the ground-state bleaching and stimulated emission (SE) overlap with the excited-state absorption (ESA) signal originating from the S_1-S_{n1} (Ref. 30) and S_2-S_{n2} (Refs. 24 and 36) transitions, and potentially also from transitions originating from the so-called S^* state, whose properties are still a matter of debate.[37–39] Despite the large number of states invoked to explain specific experiments, most results in the literature point in the direction that a model involving the S_0-S_2 and S_1-S_{n1} transitions is sufficient to explain the pump-probe spectra of carotenoids. In this scheme the initially prepared S_2 state relaxes on a ~ 100 fs time scale. The decay of the S_2 state is matched by the rise of the ESA of the S_1-S_{n1} transition that is present in the 500–650 nm spectral range (Fig. 1).

Here we present a comprehensive study of the third order optical response of astaxanthin and lycopene in tetrahydrofuran (THF). Lycopene is a linear carotenoid with $N=11$ (see Fig. 1 for structure). Astaxanthin has also eleven conjugated C=C bonds, but two of them are located in the *s-cis* orientation at terminal rings that increase conformational disorder resulting in larger inhomogeneous broadening.[40] Moreover, conjugation is extended to two carbonyl groups that usually alter excited-state properties and leads to further broadening of the linear absorption spectra.[41,42] Yet, both lycopene and astaxanthin have nearly the same energies of the vertical S_0-S_2 transition and S_1 lifetimes of 4 to 5 ps for lycopene[43] and astaxanthin.[44] They are therefore ideal for identification of influence of structural features on excited-state dynamics. In addition, the long conjugation makes both lycopene and astaxanthin good candidates for studies of potential involvement of the intermediate states in the S_2-S_1 relaxation step because both $1B_u^-$ and $3A_g^-$ states are predicted to be located between the S_2 and S_1 states.[31] Based on frequency-resolved photon echo experiments[45–47] we investigate various projections of the third-order polarization including the transient grating, the peak shift, the echo width, and the frequency-resolved transient grating. The combined analyses of the various projections allow us to develop a minimal model for the carotenoid optical response, taking into account both population dynamics and system-bath interactions. The analysis allows us to obtain the energy-gap correlation functions for the two carotenoids and investigate the relation between the structural motifs of the carotenoids and the system-bath interaction.

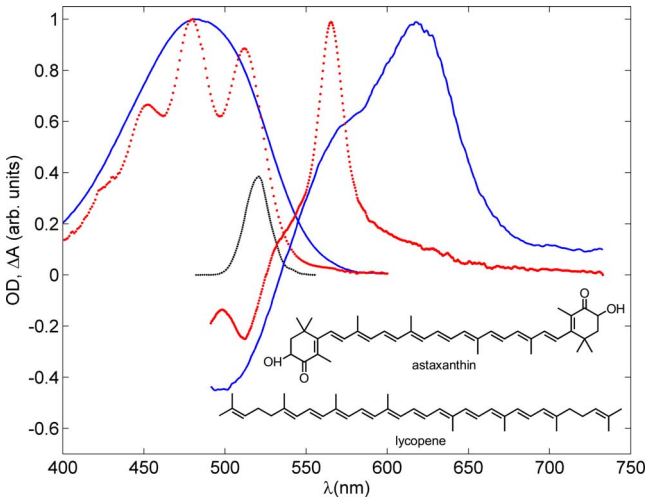

FIG. 1. (Color online) Linear absorption of astaxanthin (blue solid) and lycopene (red dot) in THF. Also shown is transient absorption signals taken at $T=1$ ps (right side of the figure) for astaxanthin (blue solid) and lycopene (red dot) in THF. The spectrum of the laser pulses centered at 520 nm is schematically shown in the figure in black dots. Inserted in the figure are the structures of the two carotenoids.

II. EXPERIMENTAL METHODS

The experimental setup for the three-pulse photon echo experiment has been described previously.[48] In brief, the output from a noncollinear amplifier is split into three pulses of approximately equal intensity and two separate delay lines are used to introduce the delay between the three pulses. The three beams are combined into a 170 μm spot by a spherical mirror. In order to increase the accuracy in the determination of the relative delay of the pulses, six two-pulse echoes are detected and used to determine the relative delays between the first two pulses, τ and the last two pulses, T. The three-pulse echoes in the $-k_1+k_2+k_3$ and $k_1-k_2+k_3$ directions are either detected by (single) diodes or sent to a 0.2 m spectrograph and measured by two diode array detectors.

The pulses used in the experiments had a Gaussian shape with a full width at half maximum (FWHM) of 17 nm and were centered at 520 nm. The temporal profiles of the pulses were characterized by second-order autocorrelation (AC) in a 25 μm BBO crystal. The resulting AC had a Gaussian shape with a FWHM of 40 fs, resulting in a time bandwidth product of 0.52. The excitation density at the sample was estimated to be 2×10^{14} photons/pulse/cm^2.

Astaxanthin, lycopene, and THF (spectroscopic grade) were purchased from Sigma-Aldrich and used without fur-

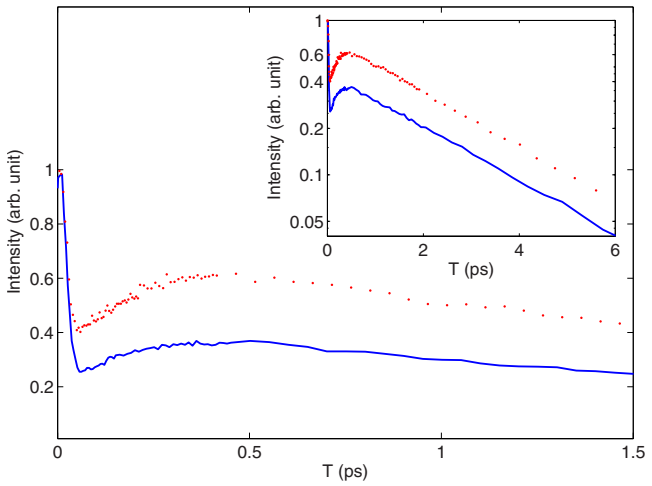

FIG. 2. (Color online) Transient grating signal for astaxanthin (blue solid) and lycopene (red dot). The inset shows the long-time decay of the signal in a logarithmic scale.

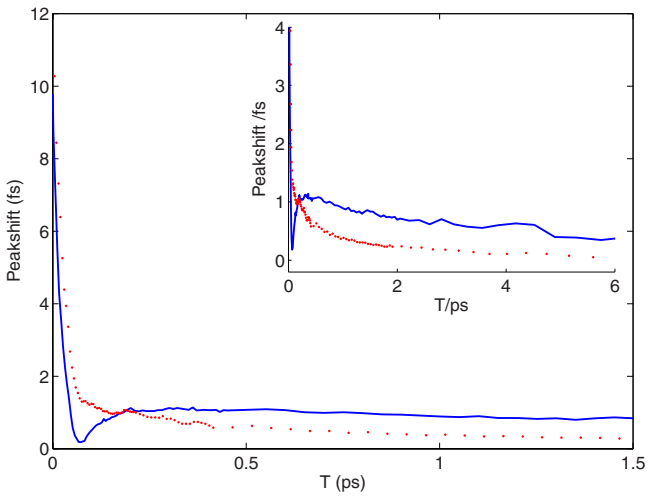

FIG. 3. (Color online) Peak shift signal as a function of population time (T) for astaxanthin (blue solid) and lycopene (red dot). The inset shows the dynamics of the peak shift on a longer time scale.

ther purification. The sample was contained in a 100 μm-thick quarts cell and both samples had an optical density of $\sim$0.15 at the excitation wavelength to avoid distortions to the echo signal.[49] The same laser pulses were used for both lycopene and astaxanthin to facilitate comparison of the results.

III. EXPERIMENTAL RESULTS

The three light-matter interactions that constitute the three-pulse photon echo sequence expand the induced polarization on three independent coordinates. Carrying out three-pulse photon echo experiments thus generates vast amounts of data and a reduction to a few selected projections is needed to analyze the results. First we focus on the two-dimensional representation of the echo intensity as a function of τ and T (i.e., integrated detection). In further dissection of this information we focus on the transient grating, the peak shift signal, and the width (FWHM) of the echo signal. For a two-level system (TLS) these three projections are, in certain limits, indicators of different aspects of the system-bath interaction and population dynamics. In the impulsive limit approximation the transient grating signal is directly related to the population dynamics.[5] The peak shift signal on the other hand is the first-order approximation to the energy-gap correlation function (henceforth denoted simply by correlation function).[5,9,10] The width of the echo signal is an indicator of the strength of the coupling between the system and the bath, both in the impulsive limit[7] and when finite pulses are used.[50] A composite analysis of all three projections of the echo signal will, thus, provide a comprehensive picture of the system-bath interaction and population dynamics.

In the transient grating projection both carotenoids show qualitatively similar behavior as shown in Fig. 2. The signal is characterized by a strong spike around $T=0$ followed by a fast decay on sub-100-fs time scale. After about 100 fs the signal recovers and continues to rise until $T=500$ fs, after which the signal decays to zero. For large T, the transient grating signal decays exponentially with a time constant of $\sim$2.6 ps in both carotenoids, corresponding to a lifetime of the S_1 state of 5.2 ps (inset of Fig. 2). In the transient grating projection the main difference between the astaxanthin and lycopene measurement is the level to which the signal recovers after the initial dynamics. A careful inspection of the rise reveals that the corresponding time constant differs between the two carotenoids, where lycopene appears to have a shorter rise time.

The peak shift signals of the two carotenoids are shown in Fig. 3. In the peak shift projections there are clear qualitative differences between the two samples. In astaxanthin the peak shift has a rapid decay followed by a node at $\sim$70 fs. The signal then recovers to about 1 fs. The inset of Fig. 3 shows that the peak shift decays slowly on a ps time scale, and at 5 ps, where the signal gets noisy due to the recovery of the ground state, the peak shift in astaxanthin is 0.3 fs. In lycopene on the other hand there is only monotonic decay of the peak shift signal. The initial peak shift in lycopene is higher compared to astaxanthin (14 and 10 fs, respectively). In contrast to astaxanthin, lycopene does not have a static component of the peak shift, and the signal decays to zero within 5 ps.

While the transient grating and the peak shift signal are sensitive to the shape and strength of the spectral density, the width of the echo signal is mostly sensitive to the reorganization energy of the modes coupled to the electronic transition.[50] From the experimental results displayed in Fig. 4, we conclude that there is a clear quantitative difference between the two carotenoids. Qualitatively however, the signals look similar; the echo widths of both carotenoids exhibit a fast recurrence on sub-100-fs time scale, after which the width settles at a static level. We find that the width of the astaxanthin signal at long population times is significantly lower compared to lycopene (35.5 and 40 fs, respectively). Thus, it can be concluded that the reorganization energy of the modes that couple to the electronic transition is larger in astaxanthin as compared to lycopene.

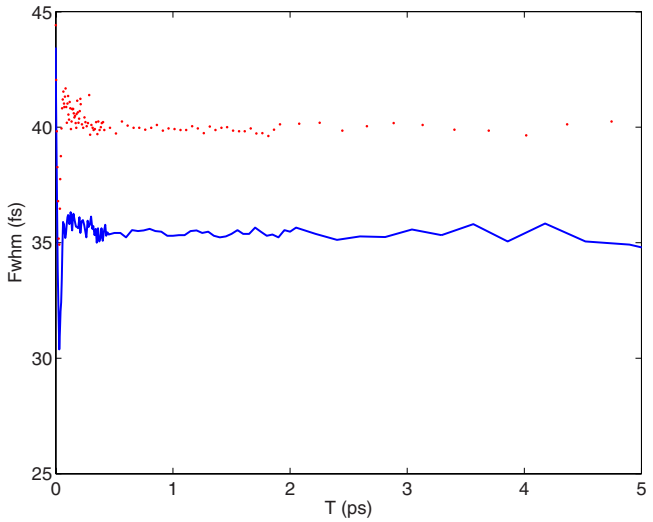

FIG. 4. (Color online) Width of the echo signal as a function of population time, T, for astaxanthin (blue solid) and lycopene (red dot).

While the two-dimensional picture of the echo intensity provided by integrated detection gives a lot of information on population and the system-bath interaction, it is relatively insensitive to the evolution of the induced polarization during the last propagation period (t). Therefore it cannot provide the complete picture of the system-bath interaction. Following the evolution during the last coherence period is of particular importance in multilevel systems where the signal is the result of interference of many different transitions. Here we have chosen to frequency resolve the signal, thereby obtaining the intensity of the Fourier transform of the polarization as a function of all three variables (time and frequencies). Figure 5 shows the spectra of the echo signal as a function of τ for $T=0$ for astaxanthin. The two phase matching directions give the same results, and here we present the

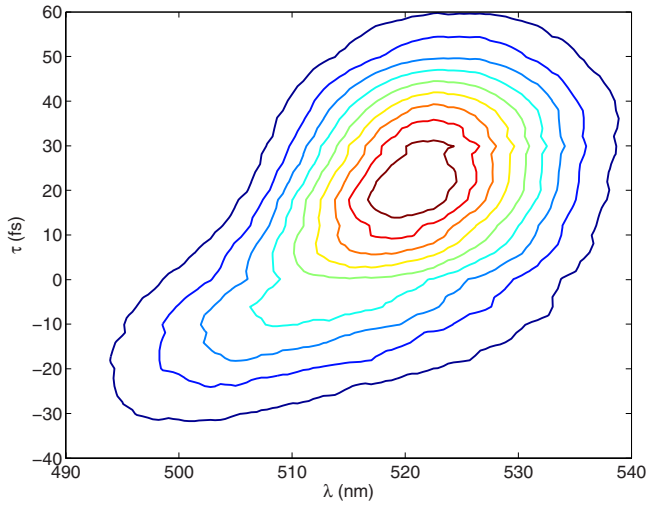

FIG. 5. (Color online) Mixed time-wavelength resolved three-pulse photon echo signal at $T=0$ for astaxanthin in THF. This image shows the average of both phase matching directions, and the signal in the $k_1-k_2+k_3$ direction has been inverted around $\tau=0$. The contours lines are at 0.9, 0.8, 0.7…0.2, 0.1, of the peak intensity.

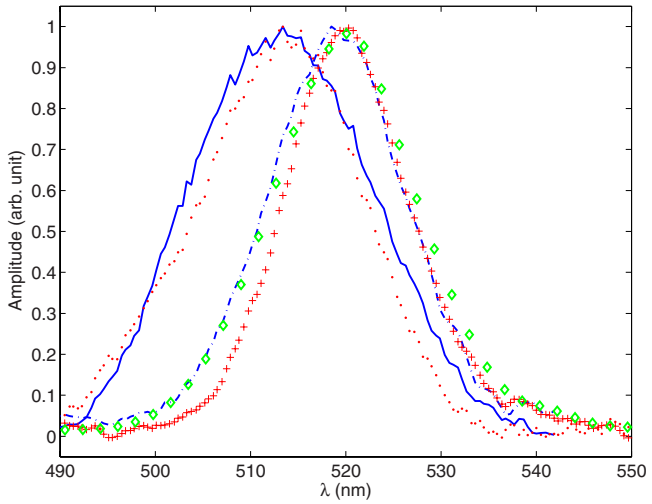

FIG. 6. (Color online) Frequency-resolved transient grating for astaxanthin (blue solid) and lycopene (red dot) at $T=0$. At longer population times ($T=3$ ps) the echo spectra and the laser spectra overlap for both astaxanthin (blue dash-dot) and lycopene (red +). All data represent the average over both phase matching directions. The spectra of the laser pulses are also shown in the figure (green diamonds).

average of the two after proper reversal of τ for the $k_1-k_2+k_3$ direction. The echo signal at positive τ matches the excitation pulse spectra, but there is a clear spectral change in going from positive to negative τ. On the nonrephasing side ($\tau<0$) we see a blueshifted echo with components that apparently lay outside the bandwidth of the pulses. This can also be seen in the frequency-resolved transient grating signal at $T=0$. The signal is significantly blueshifted compared to the laser spectrum as shown in Fig. 6. The frequency-resolved transient grating signal shows a redshift on ~50 fs time scale in both carotenoids. After about 100 fs the maxima of the echo spectra reach the central wavelength of the laser pulses. On a longer time scale the spectra of the echo narrow and converge to the spectrum of the laser pulses. Quantitatively the results for the mixed time-frequency-resolved spectra in lycopene are very similar (not shown). The similarity is underlined in the frequency-resolved transient grating signals shown in Fig. 6.

IV. MODEL

The experimental results presented in Sec. III allow us to develop a model for the population dynamics and system-bath interaction in carotenoids. Clearly the carotenoids have a more complex electronic structure then the TLS.[6] Photon echo studies with multilevel systems have shown that many of the TLS/impulsive limit approximation predictions fail when the population dynamics are taken into account.[15–17,19,20] It is also known that while the transient grating signal in the impulsive limit only probes population dynamics, it becomes sensitive to system-bath interactions as the pulses become longer.[5] In addition, the effect of finite pulses may significantly alter the appearance of the signals around the pulse overlap region as more pathways contribute

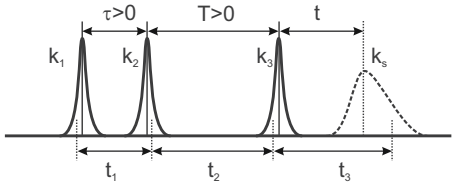

FIG. 7. Definition of time variables. τ, T, and t refers to the center of gravity of the pulse envelops, while t_1, t_2, and t_3 refers to the time when the interaction with the specific electric fields occur.

to the signal. These effects can easily be interpreted as new phenomena, even though they are inherent to the way the signals are generated. It is further expected that the pulse overlap effects are more severe in multilevel system, and it is therefore necessary to include these effects in the simulations. Here we aim to develop a generic carotenoid model that includes the system-bath interaction and population dynamics, as well as the effect of finite pulse duration. First, we raise semiquantitative arguments to formulate the minimal multilevel structure which correspond to our system. We then carry out a rigorous test of the model via comparison of our simulations with the experimental results.

The majority of experimental investigations of carotenoids have been explained using a model involving the S_0-S_2 and S_1-S_{n1} transitions. For such a model we expect that for times shorter than the lifetime of the S_2 state (sub-100 fs), it should be possible to account for the experimental observations without having to consider the S_1-S_{n1} transition. More specifically, if these transitions (S_0-S_2 and S_1-S_{n1}) constitute the minimal model to explain carotenoid signals in the visible spectral range, then a TLS description should be sufficient to model the dynamics of the frequency-resolved data shown in Figs. 5 and 6. We find however, that the TLS model is incapable of reproducing the strong blueshifted feature at negative τ for $T=0$. We have also carried out simulations including chirp of the laser pulses, but the effect of chirp is not sufficient to explain the experiments. However, when simulating the short-time dynamics with a model including the S_2-S_{n2} transition we find that we can reproduce the blueshift of the frequency-resolved transient grating signal and the very rapid shift toward red that occurs on the time scale of the pulse duration. To comply with the pump-probe results we include the S_1-S_{n1} ESA that will contribute to the signal in the spectral region accessible with our laser pulses (see Fig. 1). Our results thus point in the direction of a model containing both S_2-S_{n2} and S_1-S_{n1} ESA, as well as bleach and SE as the minimal model to explain the experimental results.

We base the theoretical description of our carotenoid model (including S_0-S_2, S_2-S_{n2}, and S_1-S_{n1} transitions) on the model developed by Brixner.[51] The third-order polarization generated in the $-k_1+k_2+k_3$ direction invoking the rotating wave approximation can be written as

$$P(\tau,T,t) = \exp(-i\omega_0 t + i\omega_0 \tau)\int_0^\infty\int_0^\infty\int_0^\infty dt_1 dt_2 dt_3 \left\{ \begin{array}{l} S_{\mathrm{R}}(t_1,t_2,t_3)\begin{bmatrix} A^*(t-\tau-t_1-t_2-t_3)A(t-T-t_2-t_3)A(t-t_3)+ \\ A^*(t-\tau-t_1-t_2-t_3)A(t-t_2-t_3)A(t-T-t_3) \end{bmatrix} \\ S_{\mathrm{NR}}(t_1,t_2,t_3)\begin{bmatrix} A(t-T-t_1-t_2-t_3)A^*(t-\tau-t_2-t_3)A(t-t_3)+ \\ A(t-t_1-t_2-t_3)A^*(t-\tau-t_2-t_3)A(t-T-t_3) \end{bmatrix} \\ S_{\mathrm{DQC}}(t_1,t_2,t_3)\begin{bmatrix} A(t-T-t_1-t_2-t_3)A(t-t_2-t_3)A^*(t-\tau-t_3)+ \\ A(t-t_1-t_2-t_3)A(t-T-t_2-t_3)A^*(t-\tau-t_3) \end{bmatrix} \end{array} \right\}, \tag{1}$$

where S_{R}, S_{NR}, and S_{DQC} denote rephasing, nonrephasing, and double quantum coherence (DQC) pathways, respectively (for definitions of time variables see Fig. 7). The product of field amplitudes in the square brackets takes care of all causality-allowed time orderings of the interaction of the system and the fields. In the case of S_{R}, the first line denotes an interaction sequence 1–2-3 (the numbers indicate the pulses) while the second line has the two last interactions permuted (1–3-2). From the last line we see that the DQC pathways, S_{DQC} are only possible when pulse 1 interacts last (ordering 2–3-1 and 3–2-1) and will only contribute in the pulse overlap region. In Eq. (1) all the information about the material response and its interaction with the surroundings is incorporated into the (summed) response functions S_{R}, S_{NR}, and S_{DQC}. The summed response functions describe qualitatively different Liouville pathways and each of these components is the sum over all Liouville pathways with similar oscillatory factors.[51]

Our simulations of the frequency-resolved data have shown that the mixed time-frequency-resolved signal depends on chirp. Our pulses have a time bandwidth product $\Delta\tau\Delta\nu=0.52$, and are not completely free of chirp. Ideally, the full information about the electric field should be included in the simulations. Here we only allow the pulses to have linear spectral chirp bound by the constraints of the measured AC and the pulse spectra (i.e., by the time bandwidth product). More details about the role of chirp in photon echo experiments will be given in a separate publication.[52]

As we have pointed out, both the S_2-S_{n2} and S_1-S_{n1} transitions are needed to model *all* our experimental data on *all* time scales. Figure 8 illustrates the energy-level structure, the

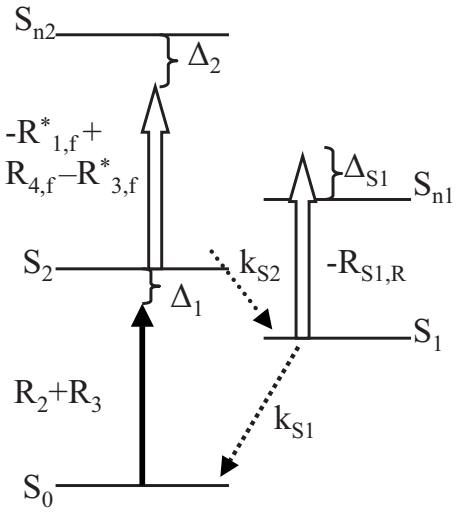

FIG. 8. The minimal model of the third-order optical response of the carotenoids. The solid arrow corresponds to TLS transitions (both bleach and stimulated emission), while the hollow arrows correspond to ESA transitions. The detuning between the different (vertical) transitions and the laser frequency is indicated in the figure. The response functions for pulse order 1-2-3 for each transition is indicated in the figure.

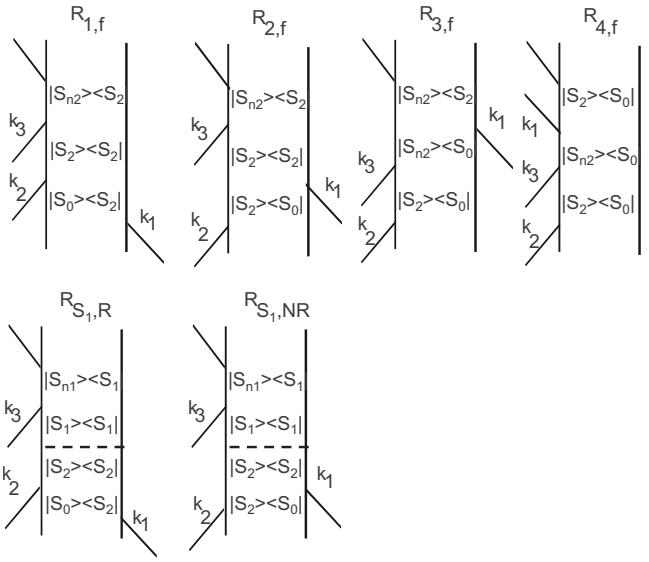

FIG. 9. Feynman diagrams showing the pathways involving ESA for the carotenoid system corresponding to the first row in the square bracket for S_R, S_{NR}, and S_{DQC} in Eq. (1). The diagrams for the second row are obtained by permutation of k_2 and k_3. The dashed line in $R_{S1,R}$ and $R_{S1,NR}$ denotes population relaxation.

relaxation pathways, and the appropriate response functions for our carotenoid model. For the S_1-S_{n1} ESA we assume that the coherence is lost during the population relaxation to the S_1 state. With this approximation we can neglect the nuclear history effect[53] and dress the response functions with population dynamics.[20,24,54] As we neglect the nuclear history effect for all states we do not need to explicitly consider the part of the population that is returning to the ground state, and we can model the recovery of the bleach via a decay of the ground-state response function R_3 and R_4.[55] For our model the expression for the response functions S_R, S_{NR}, and S_{DQC} read

$$S_R = \frac{1}{\Gamma_{S2} - \Gamma_{S1}} R_3 \{ -\Gamma_{S1} \exp(-\Gamma_{S2} t_2) + \Gamma_{S2} \exp(-\Gamma_{S1} t_2) \} \frac{-1}{\Gamma_{S2} - \Gamma_{S1}} \Gamma_{S2} R^*_{S1,R} \{ -\exp(-\Gamma_{S2} t_2) + \exp(-\Gamma_{S1} t_2) \} + (R_2 - R^*_{1,f}) \exp(-\Gamma_{S2} t_2), \quad (2)$$

$$S_{NR} = \frac{1}{\Gamma_{S2} - \Gamma_{S1}} R_4 \{ -\Gamma_{S1} \exp(-\Gamma_{S2} t_2) + \Gamma_{S2} \exp(-\Gamma_{S1} t_2) \} \frac{-1}{\Gamma_{S2} - \Gamma_{S1}} \Gamma_{S2} R^*_{S1,NR} \{ -\exp(-\Gamma_{S2} t_2) + \exp(-\Gamma_{S1} t_2) \} + (R_1 - R^*_{2,f}) \exp(-\Gamma_{S2} t_2), \quad (3)$$

$$S_{DQC} = \{ R_{4,f} - R^*_{3,f} \}, \quad (4)$$

where $\Gamma_{Sj} = T^{-1}_{Sj}$. The response functions R_1-R_4 are the same as those for a TLS,[6] while $R_{1,f}$-$R_{4,f}$ are related to the S_2-S_{n2} ESA. Finally, the $R_{S1,R}$ and $R_{S1,NR}$ response functions are associated with the S_1-S_{n1} ESA. Figure 9 shows the Feynman diagrams associated with the response functions involving the ESA transitions. The expressions for $R_{1,f}$-$R_{4,f}$ and R_{S1} are given in the Appendix. T_{S2} and T_{S1} are the lifetimes of the S_2 and S_1 states, respectively. We further assume that the relaxation from the S_1 state fills the "hole" in the ground state S_0 so that the ground-state response functions decay in concert with the disappearance of the S_1 state. The strength of each response function is controlled by the transition dipole moments of the participating transitions. The expressions for the response functions including the appropriate phase factors are given in the Appendix.

The rate of the S_2 population relaxation can be obtained from published pump-probe experiments.[43,44,56] Here we use S_2 lifetimes of 80 and 160 fs for lycopene and astaxanthin, respectively. In order to obtain a good agreement with our experiments we chose the astaxanthin lifetime which corresponds to the higher end within reported confidence limits. Our transient grating data suggest, in agreement with pump-probe experiments,[43,44] that the S_1 relaxation takes place on the same time scale in both molecules, and here we use 5.2 ps for the S_1 lifetime. The transition dipole moment for the S_2-S_{n2} ESA is taken to be the similar to the bleach transition dipole moment for both molecules, while the S_1-S_{n1} ESA transition dipole moment is taken to be slightly stronger than the bleach (see Table II). The spectral density describing the system-bath interaction is constructed from a time domain correlation function[53] containing one 40 fs Gaussian, one 100 fs exponential and one 20 ps exponential decay. The last component reflects nuclear motions occurring on a time scale comparable or slower than the lifetime of the S_1 state. The bandwidth of the pulses used in the experiments is only 620 cm^{-1}, significantly lower than the frequencies of the C-C and C=C vibrational modes. Since we do not observe any oscillations due to the vibrational modes in the transient grating or peak shift signal, we omitted these modes from the simulations of the echo signal.

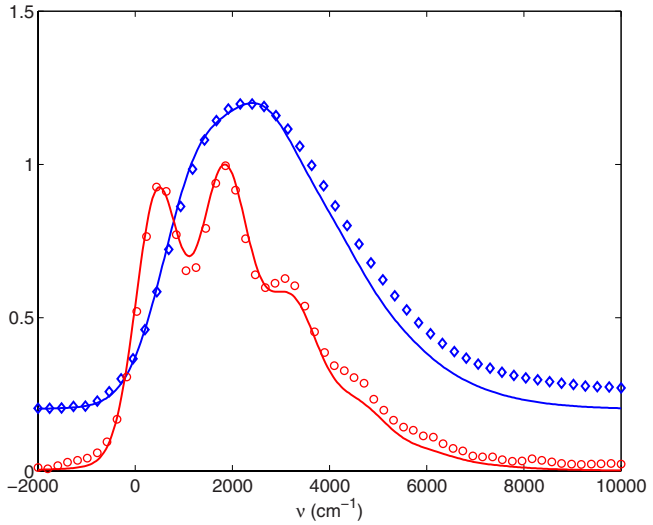

FIG. 10. (Color online) Experimental linear absorption line shape for astaxanthin (blue diamonds) and lycopene (red circles). The solid lines are simulations based on the parameters discussed in the text. The zero frequency correspond to the ZPL and is related to the vertical transition by $\upsilon = \upsilon_{\mathrm{ZPL}} + \lambda$. The ZPL is positioned at 18200 and 19 000 cm^{-1} respectively. In lycopene the ZPL is located close to the 50% rise of the red edge of the absorption spectra. The larger reorganization energy of astaxanthin shifts the ZPL further to the red in the absorption spectra and the 50% rise is at ~ 600 cm^{-1}.

To carry out the calculations with finite pulses it is necessary to set the detuning factors Δ_1, Δ_2, and Δ_3 defined in the Appendix and in Fig. 8. To set the detuning relative to the vertical transition of the S_0-S_2 transition, Δ_1, we need to simulate the linear absorption spectra. In order to simulate the absorption spectra we add two vibrational modes to the overdamped low-frequency modes of the spectral density. Taking two vibrational modes corresponding to the C-C and C=C stretches with frequencies 1150 (S=0.5) and 1520 (S=0.7) cm^{-1} we obtain a fair agreement with the vibrational progression in lycopene. We can also simulate the astaxanthin absorption spectra by taking the same parameters for the vibrational modes and only exchanging the low-frequency underdamped modes to those obtained from the echo simulations. Figure 10 shows the experimental and simulated line shapes (absorption spectra divided by frequency) for astaxanthin and lycopene. Comparing to Fig. 1 we see that for lycopene we excite close to the zero-phonon line (ZPL) and we set the detuning relative to the vertical transition to equal the reorganization energy of the spectral density (since the vertical transition energy υ obeys $\upsilon = \upsilon_{\mathrm{ZPL}} + \lambda$). In astaxanthin the ZPL is pushed further down in energy due to the larger reorganization energy and we excite higher in energy relative to the ZPL. Here we set the detuning from the vertical transition to be equal to the reorganization energy plus 300 cm^{-1}.

The detuning of the S_1-S_{n1} transition can be estimated from pump-probe experiments and here we take the vertical transitions of the S_1 ESA to ~ 625 nm and ~ 570 nm for astaxanthin and lycopene, respectively (Fig. 1). The most difficult parameter to estimate is the detuning Δ_2 of the S_2 ESA. The detuning of the S_2-S_{n2} ESA is estimated from simulations of the mixed time-frequency-resolved spectra where the blueshift of the spectra at the nonrephasing side depends on the detuning factor. The results of the simulations are summarized in Figs. 11–14, and the parameters used for the model are summarized in Tables I and II.

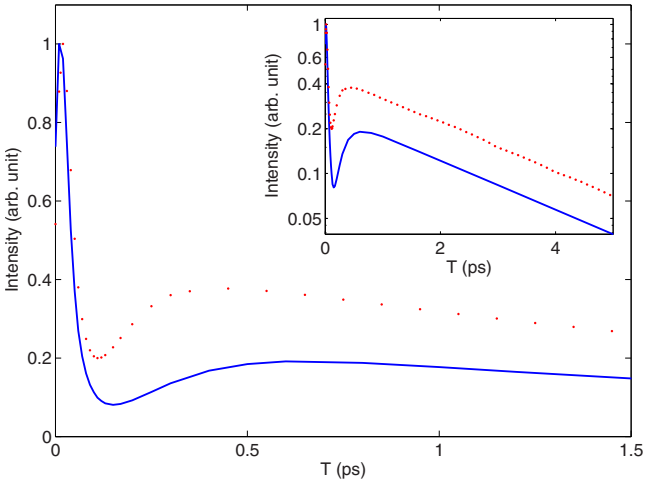

FIG. 11. (Color online) Transient grating signal for the astaxanthin model (blue solid) and the lycopene model (red dot). The inset shows the decay of the signals on ps time scale.

V. DISCUSSION

The simulations clearly show that the generic model developed for the carotenoids in Sec. IV can explain the experimental results presented in this work. With the model in place we can start to interpret the experimental results and draw conclusions about the underlying population dynamics and system-bath interactions that give rise to the observed spectroscopic signals. However, just as important as the results of the simulations (the parameters) is the development of the model. We will thus start with a discussion of how to

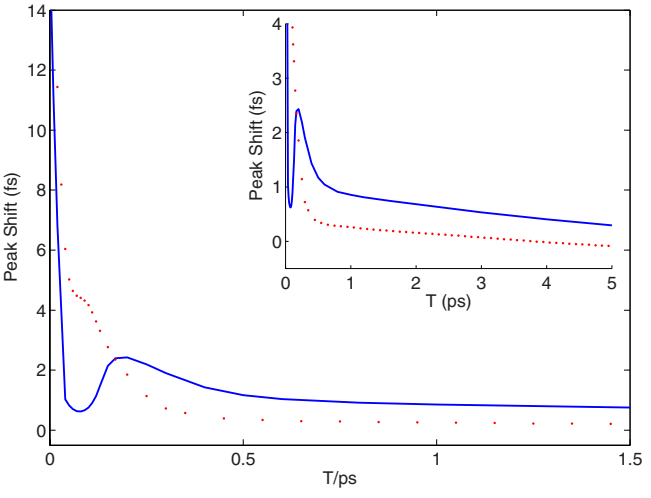

FIG. 12. (Color online) Peak shift for the astaxanthin model (blue solid) and the lycopene model (red dot).

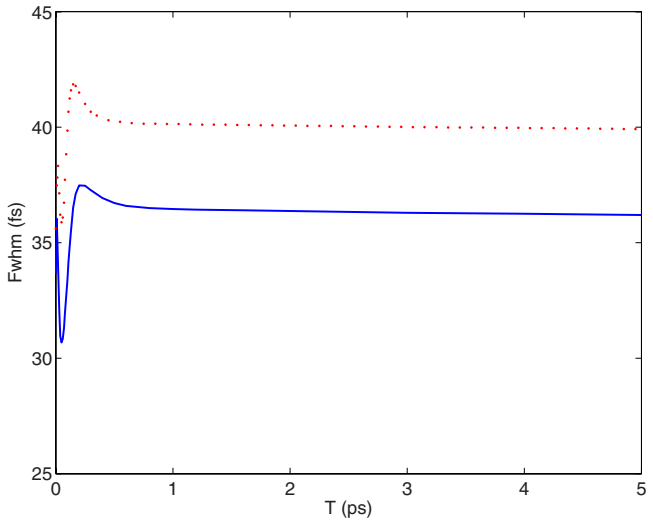

FIG. 13. (Color online) The echo width for the astaxanthin model (blue solid) and the lycopene model (red dot).

develop the model and how to use it to interpret the experimental signals.

The first step in constructing a model for the optical response of a molecule is to find the minimal description of the transitions contributing to the signals. From the integrated detection experiments it is difficult to directly determine the minimal model. In our simulations we find that all three projections used to quantify the experiments are sensitive to the presence of the S_2-S_{n2} ESA, but the differences in our simulations are not large enough to decisively conclude if the S_2-S_{n2} ESA is present or not. When examining the frequency-resolved experiments it becomes clear that the additional S_2-S_{n2} transition is needed to explain the broad spectra of the frequency-resolved transient grating signal at $T=0$ and the following rapid redshift. We find that the magnitude of the blueshift of the frequency-resolved transient grating signal at $T=0$ depends on the strength of the transition dipole moment of the S_2-S_{n2} transition. To obtain a shift of our simulated signal that agrees with the experiments we need to assume that the S_2-S_{n2} transition dipole moment is approximately equal to the bleach transition dipole moment. While such a strong transition from an excited state might seem surprising, we point out that the S_1-S_{1n} transition is also as strong as the bleach signal, and our value is by no means unreasonable. The origin of the broad blueshifted spectra at $T=0$ can be traced to the DQC pathways, which can only be reached for *inverted* ordering of the interactions with the electric field (i.e., 3–2-1) ($R_{3,f}$ and $R_{4,f}$ in Fig. 9) [see Eq. (1)]. The DQC pathways will mostly contribute for $T=0$ and at negative τ, where the probability for inverted ordering of the interactions is greatest. The DCQ pathways themselves produce a broad spectrum on the nonrephasing side of the frequency-resolved echo signal in the quasi-impulsive limit. For longer pulses the S_2-S_{n2} ESA transition selects either the high- or low-frequency side of the spectrum depending the detuning, leading to a blueshift or redshift of the signal on the nonrephasing side. Our simulations do not give a very accurate value for the detuning of the S_2-S_{n2} transition relative to the laser frequency, but we conclude that the detuning for the S_2-S_{n2} transition must be negative ($\Delta_2<0$). Since the probability for the inverted ordering of the interactions with the electric fields rapidly diminishes as T increases, we see a redshift of the signal on the same time scale as the pulse duration due to the diminishing amplitude of the DQC pathways. We point out that to simulate the frequency-resolved echo signal (like in Fig. 6) in the present case requires knowledge of three correlation functions, two detunings and two transition dipole moments. Unfortunately the response functions associated with the S_{n2} level are either overlapping with the bleach and SE contributions ($R_{1,f}$-$R_{2,f}$), or are only visible during the pulse overlap (the DCQ pathways). This makes it very difficult to obtain a clean measurement of these response functions and the underlying correlation func-

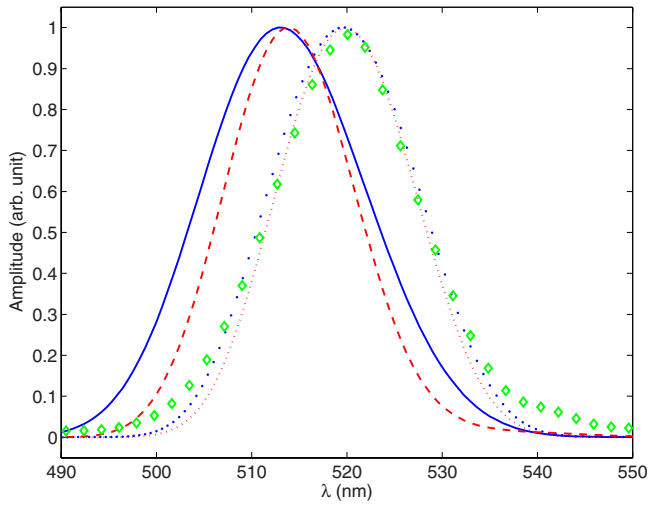

FIG. 14. (Color online) Frequency-resolved echo signal. $T=0$ for the astaxanthin model (blue solid) and the lycopene model (red dash), and at $T=3$ ps for the astaxanthin model (blue point) and the lycopene model (red dots). The experimental spectra of the laser pulses are shown in green diamonds.

TABLE I. Parameters describing the spectral density. Subscripts G and E refer to Gaussian and exponential components, respectively.

	λ_G (cm^{-1})	τ_G (ps)	λ_{E1} (cm^{-1})	τ_{E1} (ps)	λ_{E2} (cm^{-1})	τ_{E2} (ps)
Astaxanthin	350	0.04	250	0.1	750	20
Lycopene	75	0.04	250	0.1	175	20

TABLE II. The lifetimes, transition dipole strengths for the two ESA transitions, and the detunings used in the simulations. The transition dipole moments are given in units of the transition dipole moment of the bleach transition.

	T_{S2} (ps)	T_{S1} (ps)	μ_{S2}^2	μ_{S1}^2	Δ_1 (cm^{-1})	Δ_2 (cm^{-1})	Δ_3 (cm^{-1})
Astaxanthin	0.16	5.2	1	1.4	−1000	−500	3200
Lycopene	0.08	5.2	−0.8	1.4	−500	−400	1800

tions. For now we conclude that the approximation employed here, namely that the temporal dependence of the two correlation functions are the same, does not contradict our experimental results.

Having determined the transitions that contribute to the optical response in the region around $T=0$ of the photon echo experiment, we can expand our investigations to longer population times. We find that in order to reproduce the rise of the transient grating signal after ~ 100 fs we need to include the S_1-S_{n1} ESA. The previously proposed model,[24] obtained from transient grating investigations in β carotene, only invoked S_2-S_{n2} ESA to explain the results. We arrive at a different conclusion for two reasons. The first point is the treatment of the S_2-S_{n2} ESA pathway. The previously proposed model[54,57] applies the same TLS expressions for the transitions which involve S_2-S_{n2} ESA. This generates very efficient cancellation of the ESA and SE signals. It is thereby possible to create strong destructive interference between the S_2-S_{n2} ESA (negative) and the SE signal (positive). When population relaxes from the S_2 state, the echo signal becomes more positive (only bleach remaining) and the transient grating recovers. This effect has been illustrated in investigations of similar systems (with the same model but different approximation for the response functions for the ESA transition).[20,54] We use expressions for the response functions (see the Appendix) which are rigorously derived via Cumulant expansion explicitly involving ESA. In our formalism such exact cancellation of ESA and SE cannot occur for any form of the correlation functions involved. The second point to why our transient grating do not show a rise without the presence of S_1-S_{n1} transition can be found in the additional experimental input to our model. The frequency-resolved experiments give constraints to the detuning and the transition dipole moment of the S_2-S_{n2} ESA transition, further reducing the above-mentioned cancellation between SE and ESA pathways. We have not been able to reproduce a rise of the transient grating signal without incorporating the S_1-S_{n1} ESA, and we conclude that the rise of the transient grating signal does not originate from loss of destructive interference with S_2-S_{2n} ESA. The rise occurs as a consequence of the relaxation to the S_1 state and interference between the S_1-S_{n1} ESA and the remaining bleach transition. We point out that for the spectrally resolved pump-probe signal, our simulations clearly give rise to the redshifted S_1-S_{n1} state as seen in experiments (see Fig. 1). This observation further strengthens our assignment of the origin of the rise of the transient grating signal and indirectly confirms the validity of the whole model. Comparing our simulated transient grating signal (Fig. 11) with the experiments (Fig. 2) we find that the simulated transient grating signal does not rise to the same level as in the experiment. A possible explanation for this discrepancy is that our choice of line-shape function for the S_2-S_{n2} ESA transition underestimates the strength of the destructive interference in the pulse overlap region. Another possibility is that our approximations regarding the response functions for the S_1-S_{n1} transition and its correlation function are too crude, and relaxing some of these approximations may allow a better fit of the transition grating signals.

We point out that the simulation of each individual projection of the experiment (i.e., peak shift, transient grating, and width) taken alone can be improved. However, adjusting the parameters to improve the fit of one of the projections often results in qualitative disagreement with the results in the other projections. For example, if we increase the transition dipole moment of the S_1-S_{n1} transition to increase the rise of the transient grating signal, the simulated peak shift signal cannot reproduce the experiments anymore. It is thus important to model all the projections simultaneously and not to draw conclusions based on only one of the projections. We conclude this section by pointing out that a model including the S_2-S_{2n} and S_1-S_{1n} ESA transitions together with S_2 bleach and SE can account for all our experimental observations, and there are no indications that additional states are needed to describe the experiments.

The presence of a strong ESA (both S_2-S_{n2} and S_1-S_{1n}) needed to explain the transient grating (both frequency-resolved and integrated) data complicates the interpretation of the peak shift and the width of the echo signal. It is clear that the peak shift cannot be directly taken as the first-order approximation to the energy-gap correlation function as for a TLS. The very initial dynamics is masked by the interference with the S_2-S_{n2} ESA and at the intermediate time scale when all transitions contribute (~ 100 fs), the interpretation becomes even less clear. The observation that the peak shift in astaxanthin remains for very long times clearly means that the correlation function has slow decay components, but quantifying this result (by fitting the experiment) is by no means straightforward due to the interference of the bleach and the S_1-S_{n1} ESA. The rise of the peak shift in astaxanthin on ~ 100 fs time scale depends on the lifetime of S_2, but there is no direct relation between the rise time and lifetime because the rise dynamics also depends on the parameters of the spectral density. Admittedly the simulation of the shape of the node in the astaxanthin peak shift should be improved. On longer time scale our signal is the result of both the bleach and S_1-S_{n1} transition. Here we have assumed that the correlation functions for both transitions are the same and relaxing this assumption may yield better agreement between simulations and experiments. Furthermore our model makes the assumption that no memory of the fluctuations of the transition frequency survives the relaxation to a new electronic state. This postulation of incoherent relaxation affects the way we construct the S_1-S_{n1} pathway. If some of the phase memory is preserved, then the response functions of the S_1-S_{n1} pathway carries information about the phase that was acquired during the evolution in the S_2 state (i.e., the Stokes Shift). These effects are not accounted for in our model and would require some degree of correlation between the fluctuations of different electronic transitions[53] (or memory of its nuclear history). Correlated transition frequency fluctuations of different monomers has been invoked to explain the relatively slow dephasing of excitons in pigment-protein complexes[58,59] and recently in conjugated polymers.[60] To what extent correlated fluctuations of the different transitions of carotenoids exist and how they would affect the experiments remains an open question.

While our simulation of the astaxanthin peak shift is not perfect, we still capture the general features of the peak shift in both carotenoids. Most importantly, the clear node at ~ 70 fs in the peak shift of astaxanthin is absent in lycopene,

just as in the experiments. The reason why there is no recurrence in lycopene is related to the lower reorganization energy of the spectral density, the weaker influence of the slowly decaying modes, and the lower detuning of the S_1-S_{n1} ESA transition. Of these parameters, the most important is the reorganization energy of the fast modes in the spectral density. The recurrence requires a significant Stokes shift on a time scale faster than the lifetime of the S_2 state in order to occur. Examining the longer time scales of the peak shift we find that our simulations on astaxanthin also display a decay component on the order of few hundred fs that is not present in our correlation function or in our population dynamics. The amplitude and decay time of this component depends on the lifetime of the S_2 state. This component arises due to interference between the bleach and S_1-S_{n1} ESA obfuscating the TLS relation between the time scales of the spectral density and the peak shift. We further note that the slowest decay component of the simulated peak shift decays faster than our slowest mode in the correlation function (10 ps). We thus confirm the general conclusion about the multilevel systems that essentially none of the components of the peak shift can be directly interpreted as a component in the energy-gap correlation function.[17] We point out that the peak shift depends on the presence of the S_1-S_{n1} ESA and the peak shift at longer time scales depends on the R_{S1} pathways. Further work in determining the appropriate response function and correlation functions for this pathway would facilitate interpretation of the slower decay components of the S_0-S_2 energy-gap correlation function.

With the brief discussion of how the population dynamics alters the interpretation of the projections of the echo signal, we can turn to the parameters entering the simulations. More specifically we will focus on the energy-gap correlation functions for the two different carotenoids as determined from our simulations. Examining Tables I and II we see that the system-bath interaction in both carotenoids can be characterized by an energy-gap correlation function with a significant decay on 100 fs time scale followed by a slower relaxation on ps time scale. Here we have represented the fast processes by two terms in the spectral density but the exact shape of the spectral density is difficult to uncover due to the complicated interference of all transitions on ~100 fs time scale. The most striking differences between the correlation functions associated with the two carotenoids is, however, not in the time scales of the correlation function but in the magnitude of the coupling strength of the overdamped nuclear motions. This difference is illustrated in the frequency representation of the spectral density shown in Fig. 15. From the width of the experimental photon echo signal we can directly conclude that the total system-bath coupling strength is larger in astaxanthin. The width of the photon echo signal is an indicator of the total coupling strength of the system-bath interaction and it is essentially insensitive to the distribution of the modes. The increase in the coupling to slow modes can be explained by the presence of the rings at the end of the polyene backbone that contribute to the nuclear motions on a slower time scale due to steric interactions.[40] Due to the short lifetime of the S_1 state our model is quite insensitive to exact time scale of these motions and here we have set it to 20 ps, but it may be longer. We point out that the same time

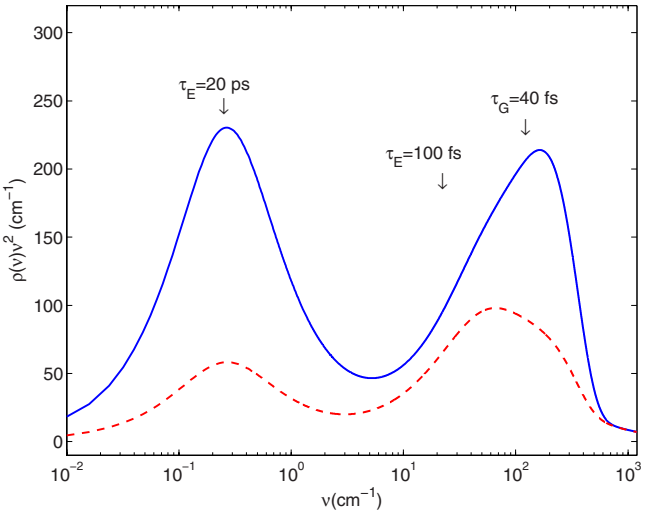

FIG. 15. (Color online) The spectral density used in the simulations for astaxanthin (blue solid) and lycopene (red dash). The origin of each component of the spectral density is indicated in the figure.

scale is present for lycopene, where the rings are absent. From studies of solvation of dye molecules it is known that the solvent reorients to minimize the free energy of the combined solvent solute system following excitation and this process shows components on ps time scale.[11] While the time scales of the correlation functions obtained for lycopene and PERY (Ref. 11) are similar, we find that both the slow and the fast mode have significantly higher reorganization energy for lycopene in THF. This can be seen as an indication that a significant part of the reorganization energy of the bath is related to solute or solute-solvent specific interactions. Clarifying the origin of these nuclear motions would require measurements in more solvents and will be left for future work. Whatever the origin of these modes, we expect this contribution to be similar for both carotenoids due to the common carbon backbone, and the role of the structural motifs should manifest themselves as the difference in the spectral densities.

From the peak shift simulations we find that the increase in the reorganization energy of the slow modes is not sufficient to explain the difference between astaxanthin and lycopene. For the node in the peak shift to occur a significant Stokes shift on the time scale of the S_2 lifetime is needed. Pinpointing the origin of this increase in reorganization energy of high-frequency modes is difficult given the single solvent measurement, but a few possibilities based on the structure can be considered. In astaxanthin the terminal rings contain both hydroxyl and carbonyl groups. The hydroxyl groups may add a fast solvation component due to its ability to form hydrogen bonds with the solvent. However, the carbonyl groups participate in the extended conjugated system meaning that these groups will couple more strongly to the electronic transition making them a likely candidate for the observed effects. The polar nature of the carbonyl group could lead to additional solvation as a response to excitation by the laser pulses. The carbonyl group will interact with the moderately polar solvent THF and increase the reorganiza-

tion energy by a polar solvation mechanism. But the carbonyl group should also feel a component of nonpolar solvation due to its high exposure to the solvent. Experimental investigations of solvation has established that polar[13,61] and nonpolar[11] solvations take place on the same time scale, with components ranging from fs to ns. Disentangling the contributions from polar and nonpolar solvation mechanisms is beyond the scope of this paper, but the developed model would be valuable for the interpretation of such studies. Comparing the results presented in this work to a full analysis of a photon echo experiment of astaxanthin in methanol and acetonitrile would allow for a more detailed picture of the importance of hydrogen bonding and the polar solvation mechanism in altering the system-bath interaction.

The role of the structural motifs in altering the system-bath interaction as reported here raises the question if these trends can be observed in other carotenoids. In this respect it is interesting to extrapolate our results to β carotene, an eleven double bond carotenoid that lacks the carbonyl and hydroxyl groups on the terminal rings but otherwise is structurally similar to astaxanthin. In terms of vibrational structure of the linear absorption spectra, β carotene is somewhere in between astaxanthin and lycopene. We would thus interpret the trend of decreasing vibrational structure from lycopene to β carotene as an increase of slow nuclear motions due to the presence of the terminal rings in β carotene. The further decrease of vibrational structure in astaxanthin would be the results of additional fast fluctuations of the energy-gap provided by the functional groups on the terminal rings.

The finding that the functional groups of astaxanthin lead to a stronger system-bath coupling has further implications. From the theory of nonadiabatic transitions,[62–64] we know that the transition rate is proportional to the spectral density of the modes involved in the nonadiabatic coupling. When the difference in energy between the states is much larger then the characteristic frequency of the bath, multiple bath quanta are needed to ensure conservation of energy in the relaxation step. In this limit an exponential dependence of the relaxation rate on the energy gap is obtained.[65] Besides the dependence on the energy gap the relaxation rate will depend on the strength of the spectral density. For the transfer from the S_2 to the S_1 state, the relevant modes are those which modulate the S_1-S_2 energy gap (not the S_0-S_2 gap as investigated in this article) and we do not have any direct information about their spectral density. However, since we relate the system-bath interaction with general structural motifs, it would be highly surprising if the S_0-S_2 and S_2-S_1 energy-gap correlation functions would show opposite trends with respect to the structural motifs. We thus expect that the spectral density describing the nonadiabatic coupling would be qualitatively similar to the spectral density determined in this paper. Since the energy gap for lycopene and astaxanthin is similar, we would predict a shorter lifetime of the S_2 state for astaxanthin due to the stronger system-bath coupling. As discussed above, we would also predict that β carotene has a stronger coupling compared to lycopene and would, given the similarity of the energy gap,[30] consequently show a faster S_2 relaxation. The nonabdiabatic theory thus predicts the S_2 lifetimes for the three carotenoids in increasing order for astaxanthin, β carotene and lycopene. Experimentally however, we find that the trend of the S_2 lifetimes is the opposite. Clearly the shortest S_2 lifetime has lycopene (80 fs) (Ref. 56) followed by β carotene (120–150 fs) (Refs. 66 and 67) and astaxanthin, (140–160 fs).[44] This apparent contradiction indicates that the S_2 to S_1 transition is not a simple nonadiabatic hopping between states, but corresponds to an almost adiabatic passage through the conical intersection where the system-bath interaction takes the role of friction. In this case the stronger system-bath interaction and higher spectral density corresponds to slower dynamics and longer lifetimes. The results on the S_2-S_1 relaxation rate in β carotene and its derivatives with varying conjugation length[66,67] raises further questions about the applicability of the nonadiabatic coupling to describe the relaxation and the use of the resulting band-gap laws to predict energy levels or relaxation rates. We point out that the existence of the band-gap law does not imply a weak-coupling limit, since the same dependence may occur for conical intersections due to the interplay of increasing energy gap with changes in the shifts between the potentials,[68] or even due to vibrational relaxation.[65]

Direct investigations of the relations between carotenoid structure and the correlation function describing the S_2-S_1 energy gap would allow a more detailed discussion of the relaxation process and the role of the conical intersection in the excited-state dynamics of carotenoids.

VI. SUMMARY

In this paper we have developed a model for the third-order spectroscopy of carotenoids including population and system-bath interactions. Our experiments show that ESA from both S_2 and S_1 needs to be taken into account to model the experimental results. The model has been applied to gain insight to the relation between the structure of the carotenoid and the system-bath interaction. We have found that the presence of the terminal rings on the polyene backbone give rise to a dramatic increase in the reorganization energy of the low-frequency modes of the spectral density. When comparing astaxanthin (rings) and lycopene (linear) we also find that the fast modes, on a 100 fs time scale, are enhanced for astaxanthin. We propose that the increase in the slow modes originate from the terminal rings while the increase in the fast modes is related to the functional groups present on the terminal rings.

ACKNOWLEDGMENTS

The corresponding author would like to thank T. Mančal at Charles University in Prague for valuable discussion regarding the modeling and for providing the corrected expressions for the response functions $R_{1,f}$-$R_{4,f}$. We also acknowledge the work of T. Pascher at Lund University in adapting the software for the frequency-resolved measurements. T.P. thanks for financial support from the Czech Ministry of Education (Grants No. MSM6007665808 and No. AV0Z50510513) and the Grant Agency of the Czech Academy of Sciences (Grant No. IAA608170604). Financial support for this work was provided by the Swedish Research

Council (VR), Knut and Alice Wallenberg foundation and the Karl Trygger foundation.

APPENDIX

In a three-level system additional response functions are needed to describe the third-order optical response. Due to a typographical error in Ref. 51 we give the complete equations here. Here we denote the electronic levels by g, e, and f in increasing order of energy. The Feynman diagrams and the corresponding response functions for the two level transitions are abundant in the literature,[6] and here we only give the expressions for the response functions involving the ESA transition. The second-order cumulant expansion for the propagators corresponding to the Feynman diagrams in Fig. 7 reads

$$R_{1,f}^{*} = (|\mu_{eg}||\mu_{ef}|)^2 \exp\{-i\Delta_1 t_1 + i\Delta_2 t_3\} \exp\begin{Bmatrix} -g_{ee}^{*}(t_1) - g_{ee}(t_2) + g_{ef}(t_2) - g_{ee}(t_3) + 2\cdot g_{ef}(t_3) \\ -g_{ff}(t_3) + g_{ee}^{*}(t_1+t_2) - g_{ef}^{*}(t_1+t_2) + g_{ee}(t_2+t_3) \\ -g_{ef}(t_2+t_3) - g_{ee}^{*}(t_1+t_2+t_3) + g_{ef}^{*}(t_1+t_2+t_3) \end{Bmatrix}, \tag{A1}$$

$$R_{2,f}^{*} = (|\mu_{eg}||\mu_{ef}|)^2 \exp\{i\Delta_1 t_1 + i\Delta_2 t_3\} \exp\begin{Bmatrix} -g_{ee}(t_1) + g_{ee}^{*}(t_2) - g_{ef}^{*}(t_2) - g_{ee}(t_3) + 2\cdot g_{ef}(t_3) \\ -g_{ff}(t_3) - g_{ee}(t_1+t_2) + g_{ef}(t_1+t_2) - g_{ee}^{*}(t_2+t_3) \\ +g_{ef}^{*}(t_2+t_3) + g_{ee}(t_1+t_2+t_3) - g_{ef}(t_1+t_2+t_3) \end{Bmatrix}, \tag{A2}$$

$$R_{3,f}^{*} = (|\mu_{eg}||\mu_{ef}|)^2 \exp\{i\Delta_1 t_1 + i\Delta_2 t_3 + i(\Delta_1+\Delta_2)t_2\} \exp\begin{Bmatrix} -g_{ee}(t_1) + g_{ef}(t_1) + g_{ee}(t_2) - g_{ef}(t_2) \\ -g_{ee}^{*}(t_3) + g_{ef}^{*}(t_3) - g_{ee}(t_1+t_2) - \\ g_{ee}(t_2+t_3) + 2\cdot g_{ef}(t_2+t_3) - g_{ff}(t_2+t_3) \\ +g_{ee}(t_1+t_2+t_3) - g_{ef}(t_1+t_2+t_3) \end{Bmatrix}, \tag{A3}$$

$$R_{4,f} = (|\mu_{eg}||\mu_{ef}|)^2 \exp\{i\Delta_1(t_1+t_2+t_3) + i\Delta_2 t_2\} \exp\begin{Bmatrix} -g_{ee}(t_1) + g_{ef}(t_1) - g_{ee}(t_2) + 2g_{ef}(t_2) \\ -g_{ff}(t_2) - g_{ee}(t_3) + g_{ef}(t_3) + g_{ee}(t_1+t_2) \\ -g_{ef}(t_1+t_2) + g_{ee}(t_2+t_3) - g_{ef}(t_2+t_3) \\ -g_{ee}(t_1+t_2+t_3) \end{Bmatrix}, \tag{A4}$$

where the detuning factors between the laser field and the response function are

$$\Delta_1 = \omega_0 - \omega_{eg},$$

$$\Delta_2 = \omega_0 + \omega_{ef} = \dot{\omega}_0 - \omega_{fe}. \tag{A5}$$

The ground-state response functions can be found in the literature.[6] The phase factors for the ground-state response functions have the same form as for $R_{1,f}$-$R_{4,f}$ with the substitution $\Delta_2 = \Delta_1$. Equations (A1)–(A3) contains three different line-shape functions g_{ee}, g_{ef}, and g_{ff}. These line-shape functions are determined by the energy-gap correlation functions for the involved transitions. The g_{ee} line-shape function is the same as for the TLS and depends on the fluctuation of the energy gap of the bleach transition, while the g_{ff} depends on the fluctuations of the S_0-S_{n2} transition. The off-diagonal line-shape function g_{ef} depends on the correlation between the fluctuations of the different transitions. Little is known about the time dependence of the off-diagonal correlation functions and here we assume them to have the same temporal dependence as the (ground-state) correlation function. Here we assume that the additional line-shape functions are related to the ground-state line-shape function via a simple relation

$$g_{ef}(t) = \frac{1}{2} g_{ee}(t),$$

$$g_{ff}(t) = \frac{1}{2} g_{ee}(t). \tag{A6}$$

Due to the population dynamics in the system a three-level model is not sufficient to describe the experimental data. In addition, we need to include the pathways that include ESA from the S_1 state. If coherence is completely lost during the population transfer, only the evolution during t_1 and t_3 should affect the response function. As the response function for the S_1-S_{n1} ESA transition we use

$$R_{S1,\mathrm{R}} = |\mu_{eg}|^2 |\mu_{S1}|^2 \times \exp\{-i\Delta_1 t_1 + i\Delta_{S1} t_3\} \exp\{-g_{ee}^{*}(t_1) - g_{S1S1}(t_3)\}, \tag{A7}$$

$$R_{S1,\mathrm{NR}} = |\mu_{eg}|^2 |\mu_{S1}|^2 \times \exp\{i\Delta_1 t_1 + i\Delta_{S1} t_3\} \exp\{-g_{ee}(t_1) - g_{S1S1}(t_3)\},$$

$$\Delta_{S1} = \omega_0 - \omega_{S1}. \tag{A8}$$

Here an additional line-shape function appears (g_{S1S1}). The g_{S1S1} line-shape function depends the fluctuations of the S_1-S_{n1} ESA transition frequency (analogous to the line-shape function for the ground-state transition). The simple form of this response function leads to a simple interpretation of the pump-probe spectra of the S_1-S_{n1} transition. In the impulsive limit the S_1-S_{n1} pump-probe spectra would reflect the Fourier transform of the decay of $\exp(-g_{S1S1})$.

The pump-probe spectra shown in Fig. 1 both indicate that the ESA spectra of lycopene and astaxanthin are narrower than the corresponding bleach signal. Here we for simplicity assume that the line-shape function $g_{S1S1}=g_{ee}$. While this choice of line-shape function cannot reproduce the details of the pump-probe signal, we find that it is sufficient to describe our experimental results. A fit of the relaxed pump-probe spectra would allow us to estimate this correlation function [and the response functions (11) and (12)] and reduce the uncertainty in the other parameters in the simulations. However, it is well known that it is in general not possible to obtain the correlation function directly from the absorption spectra. Consequently even this procedure would be hampered by some uncertainty. To fully determine the correlation function for the S_1-S_{n1} transition one should perform a photon echo experiment on the S_1-S_{n1} transition after having populated the S_1 state via relaxation from S_2.

[1] D. A. Farrow, A. Yu, and D. M. Jonas, J. Chem. Phys. **118**, 9348 (2003).
[2] T. Brixner, J. Stenger, H. M. Vaswani, M. Cho, R. E. Blankenship, and G. R. Fleming, Nature (London) **434**, 625 (2005).
[3] W. P. de Boeij, M. S. Pshenichnikov, and D. A. Wiersma, Annu. Rev. Phys. Chem. **49**, 99 (1998).
[4] G. R. Fleming and M. H. Cho, Annu. Rev. Phys. Chem. **47**, 109 (1996).
[5] T. H. Joo, Y. W. Jia, J. Y. Yu, M. J. Lang, and G. R. Fleming, J. Chem. Phys. **104**, 6089 (1996).
[6] S. Mukamel, *Principles of Non-linear Optical Spectroscopy* (Oxford University Press, New York, 1995).
[7] W. P. deBoeij, M. S. Pshenichnikov, and D. A. Wiersma, J. Phys. Chem. **100**, 11806 (1996).
[8] C. J. Bardeen, S. J. Rosenthal, and C. V. Shank, J. Phys. Chem. A **103**, 10506 (1999).
[9] M. H. Cho, J. Y. Yu, T. H. Joo, Y. Nagasawa, S. A. Passino, and G. R. Fleming, J. Phys. Chem. **100**, 11944 (1996).
[10] W. P. de Boeij, M. S. Pshenichnikov, and D. A. Wiersma, Chem. Phys. Lett. **253**, 53 (1996).
[11] D. S. Larsen, K. Ohta, and G. R. Fleming, J. Chem. Phys. **111**, 8970 (1999).
[12] S. A. Passino, Y. Nagasawa, and G. R. Fleming, J. Chem. Phys. **107**, 6094 (1997).
[13] N. Christensson, B. Dietzek, A. Yartsev, and T. Pullerits, Chem. Phys. (to be published).
[14] B. Dietzek, N. Christensson, T. Pascher, T. Pullerits, and A. Yartsev, J. Phys. Chem. B **111**, 5396 (2007).
[15] R. Agarwal, M. Yang, Q. H. Xu, and G. R. Fleming, J. Phys. Chem. B **105**, 1887 (2001).
[16] R. Jimenez, F. van Mourik, J. Y. Yu, and G. R. Fleming, J. Phys. Chem. B **101**, 7350 (1997).
[17] B. M. Cho, C. F. Carlsson, and R. Jimenez, J. Chem. Phys. **124**, 144905 (2006).
[18] T. E. Dykstra, V. Kovalevskij, X. J. Yang, and G. D. Scholes, Chem. Phys. **318**, 21 (2005).
[19] R. Jimenez, D. A. Case, and F. E. Romesberg, J. Phys. Chem. B **106**, 1090 (2002).
[20] R. Jimenez and F. E. Romesberg, J. Phys. Chem. B **106**, 9172 (2002).
[21] G. D. Scholes, D. S. Larsen, G. R. Fleming, G. Rumbles, and P. L. Burn, Phys. Rev. B **61**, 13670 (2000).
[22] X. J. Yang, T. E. Dykstra, and G. D. Scholes, Phys. Rev. B **71**, 045203 (2005).
[23] M. Sugisaki, M. Fujiwara, K. Yanagi, R. J. Cogdell, and H. Hashimoto, Photosynth. Res. **95**, 299 (2008).
[24] M. Sugisaki, K. Yanagi, R. J. Cogdell, and H. Hashimoto, Phys. Rev. B **75**, 155110 (2007).
[25] T. Siebert, V. Engel, A. Materny, W. Kiefer, and M. Schmitt, J. Phys. Chem. A **107**, 8355 (2003).
[26] M. Fujiwara, K. Yamauchi, M. Sugisaki, A. Gall, B. Robert, R. J. Cogdell, and H. Hashimoto, Phys. Rev. B **77**, 205118 (2008).
[27] J. Hauer, T. Buckup, and M. Motzkus, J. Phys. Chem. A **111**, 10517 (2007).
[28] T. Hornung, H. Skenderovic, and M. Motzkus, Chem. Phys. Lett. **402**, 283 (2005).
[29] *Carotenoid Handbook*, edited by G. Britton, S. Liaaen-Jensen, and H. Pfander (Birkhauser Verlag, Basel, 2004).
[30] T. Polivka and V. Sundstrom, Chem. Rev. **104**, 2021 (2004).
[31] Y. Koyama, F. S. Rondonuwu, R. Fujii, and Y. Watanabe, Biopolymers **74**, 2 (2004).
[32] C. M. Marian and N. Gilka, J. Chem. Theory Comput. **4**, 1501 (2008).
[33] D. W. McCamant, J. E. Kim, and R. A. Mathies, J. Phys. Chem. A **106**, 6030 (2002).
[34] S. Shim and R. A. Mathies, J. Phys. Chem. B **112**, 4826 (2008).
[35] D. Kosumi, M. Komukai, M. Yoshizawa, and H. Hashimoto, Phys. Rev. Lett. **95**, 213601 (2005).
[36] E. Papagiannakis, I. H. M. van Stokkum, M. Vengris, R. J. Cogdell, R. van Grondelle, and D. S. Larsen, J. Phys. Chem. B **110**, 5727 (2006).
[37] C. C. Gradinaru, J. T. M. Kennis, E. Papagiannakis, I. H. M. van Stokkum, R. J. Cogdell, G. R. Fleming, R. A. Niederman, and R. van Grondelle, Proc. Natl. Acad. Sci. U.S.A. **98**, 2364 (2001).
[38] D. M. Niedzwiedzki, J. O. Sullivan, T. Polivka, R. R. Birge, and H. A. Frank, J. Phys. Chem. B **110**, 22872 (2006).
[39] T. Buckup, J. Savolainen, W. Wohlleben, J. L. Herek, H. Hashimoto, R. R. B. Correia, and M. Motzkus, J. Chem. Phys. **125**,

194505 (2006).
[40] R. L. Christensen, M. Goyette, L. Gallagher, J. Duncan, B. DeCoster, J. Lugtenburg, F. J. Jansen, and I. van der Hoef, J. Phys. Chem. A **103**, 2399 (1999).
[41] H. A. Frank, J. A. Bautista, J. Josue, Z. Pendon, R. G. Hiller, F. P. Sharples, D. Gosztola, and M. R. Wasielewski, J. Phys. Chem. B **104**, 4569 (2000).
[42] D. Zigmantas, R. G. Hiller, F. P. Sharples, H. A. Frank, V. Sundstrom, and T. Polivka, Phys. Chem. Chem. Phys. **6**, 3009 (2004).
[43] H. H. Billsten, D. Zigmantas, V. Sundström, and T. Polívka, Chem. Phys. Lett. **355**, 465 (2002).
[44] R. P. Ilagan, R. L. Christensen, T. W. Chapp, G. N. Gibson, T. Pascher, T. Polivka, and H. A. Frank, J. Phys. Chem. A **109**, 3120 (2005).
[45] L. D. Book and N. F. Scherer, J. Chem. Phys. **111**, 792 (1999).
[46] L. Van Dao, J. Lumin. **106**, 243 (2004).
[47] L. Van Dao, C. Lincoln, M. Lowe, and P. Hannaford, J. Chem. Phys. **120**, 8434 (2004).
[48] B. Dietzek, N. Christensson, P. Kjellberg, T. Pascher, T. Pullerits, and A. Yartsev, Phys. Chem. Chem. Phys. **9**, 701 (2007).
[49] N. Christensson, B. Dietzek, T. Pascher, A. Yartsev, and T. Pullerits, Chem. Phys. Lett. **457**, 106 (2008).
[50] N. Christensson, B. Dietzek, A. Yartsev, and T. Pullerits, J. Chem. Phys. **130**, 024510 (2009).
[51] T. Brixner, T. Mancal, I. V. Stiopkin, and G. R. Fleming, J. Chem. Phys. **121**, 4221 (2004).
[52] N. Christensson, A. Yartsev, and T. Pullerits (unpublished).
[53] M. Yang, K. Ohta, and G. R. Fleming, J. Chem. Phys. **110**, 10243 (1999).
[54] J. Stenger, D. Madsen, P. Hamm, E. T. J. Nibbering, and T. Elsaesser, J. Phys. Chem. A **106**, 2341 (2002).
[55] Q. H. Xu and G. R. Fleming, J. Phys. Chem. A **105**, 10187 (2001).
[56] G. Cerullo, D. Polli, G. Lanzani, S. De Silvestri, H. Hashimoto, and R. J. Cogdell, Science **298**, 2395 (2002).
[57] J. Stenger, D. Madsen, P. Hamm, E. T. J. Nibbering, and T. Elsaesser, Phys. Rev. Lett. **87**, 027401 (2001).
[58] G. S. Engel, T. R. Calhoun, E. L. Read, T. K. Ahn, T. Mancal, Y. C. Cheng, R. E. Blankenship, and G. R. Fleming, Nature (London) **446**, 782 (2007).
[59] H. Lee, Y. C. Cheng, and G. R. Fleming, Science **316**, 1462 (2007).
[60] E. Collini and G. D. Scholes, Science **323**, 369 (2009).
[61] M. L. Horng, J. A. Gardecki, A. Papazyan, and M. Maroncelli, J. Phys. Chem. **99**, 17311 (1995).
[62] V. May and O. Kuhn, *Charge and Energy Transfer Dynamics in Molecular Systems* (Wiley, Berlin, 1999).
[63] R. Englman and J. Jortner, Mol. Phys. **18**, 145 (1970).
[64] K. F. Freed and J. Jortner, J. Chem. Phys. **52**, 6272 (1970).
[65] A. Nitzan, S. Mukamel, and J. Jortner, J. Chem. Phys. **63**, 200 (1975).
[66] D. Polli, G. Cerullo, G. Lanzani, S. De Silvestri, K. Yanagi, H. Hashimoto, and R. J. Cogdell, Phys. Rev. Lett. **93**, 163002 (2004).
[67] D. Kosumi, K. Yanagi, R. Fujii, H. Hashimoto, and M. Yoshizawa, Chem. Phys. Lett. **425**, 66 (2006).
[68] W. Fuss, Y. Haas, and S. Zilberg, Chem. Phys. **259**, 273 (2000).